*Southern Journal of Engineering & Technology – Special Issue, Vol. 01, Issue 01, 2024*

# Analysis of the effect of Secondary Corrugation in Self-Supporting Double Corrugated Arched Roofing System

**Tauqeer Ahmad Jan, Muhammad Aslam, Muhammad Khurram Shahzad, Muhammad Umair Akram, Talha Sattar, Ateeb Muhammad Ali, Adil Nawaz**

Department of Civil Engineering and Applied Technology, Institute of Southern Punjab (ISP) Multan, Pakistan

**Abstract**. Double corrugated arched roofing, commonly known as K-Span roofing, is a self-supporting frame-less roofing system, made up of cold formed steel sheet profile. Cold formed steel sheet is bent into different types of main profiles like rectangular and trapezoidal with a thickness of around 0.6 mm to 1.5 mm. The main profile, generally called primary corrugations, are the converted into arch shape by making transverse corrugations, these transverse corrugations are the secondary corrugations. These transverse corrugations make the use of available design standard for cold formed steel difficult. The lack of proper scientific bases and available design standards make the designer to use common design practice and general information during designing of such structure. This may lead to under design the structure, because secondary corrugations reduce the actual load carrying capacity of main profile due to discontinuity in load path, and this can lead to failure and even collapse of structure. The study aims to analyses the effect of shape modification of secondary corrugation on the load carrying capacity of the arch. In the initial part of the study actual k-span samples of different diameter were modelled on ANSYS to check to draw the comparative analysis of their load carrying capacity with straight section. Secondly, some modifications were done in shape of secondary corrugation by varying the top, bottom widths and depth according to diameter. In coherence to previous researches the secondary corrugation resulted in reduction of load carrying capacity. However, as the diameter of k-span increase the load carrying capacity of the profile increases. Where, the secondary corrugation with Trapezoidal shape having lower depth with an internal angle in a manner that makes it closer to rectangular shape, proved to be best shape for secondary corrugation.

**Keywords**: K-Span, Double corrugated sheet, Self-supporting arched roofing, transverse corrugations, numerical analysis.

**Email:** tauqeer.engr@outlook.com

## 1. Introduction

K-Span Arched Roof or self-supporting frameless double corrugated arched roofing system is utilized in buildings designed for various purposes. The supporting element of the system is made of double corrugated, high profiled trapezoid, rectangular, or other steel sheets with a core thickness ranging from 0.6 mm to 1.5 mm, profiled to form a circular arch with a span of up to 36 m. A mobile rolling mill creates each profile at site from a single steel sheet. By combining and merging profiles of different cross-sections, such as trapezoids or rectangles, a continuous cylindrical surface is produced as shown in figure 1. Roll forming causes deep corrugates to develop on the profile surface (Artur Piekarczuka, 2019) (Li Wu, 2006) (Robert Cybulski a, 2014). These panels have two corrugations: a primary corrugation that is created during the cross-section formation and a secondary corrugation that is created when the panel bends into an arch. (A. Piekarczuk, 2021). With this roofing method, steel sheets are cold formed into corrugated arch panels, which are then combined one by one to create a continuous roof free of any structural frame. Double corrugated steel arch panels addressed two crucial issues: the structure needed to have an arched roof to ensure proper rigidity and load carrying capacity, and it needed to be simple and quick to install. The goal of the system development was to create

a structure that would be economical to manufacture and simple to install. This method underwent significant modifications resulting in the development of self-supporting arch structures composed of double corrugated sheets, currently recognized as K-span. A historical image of a Quonset Hut system facility mounting from 1942 is shown in Figure-2, together with a mounting of a modern K-span facility (A. Piekarczuk, 2021).

**Figure 1: K-Span Structure (Artur Piekarczuka, 2019)**

**Figure 2. Quonset Hut for Military (A. Piekarczuk, 2021)**

K-span has been in use in the international building industry for about 80 years. Its popularity is due to its straightforward design, as well as its benefits in terms of functionality and cost. These days, on-site mobile rolling machines are used to create arch components, significantly speeding up the construction process (D. Zhadanov, 2015).

The ease of erection and speed of k-span structures is one of its greatest features. The majority of the structural elements required can be made on site. The roll-forming equipment is mobile. When compared to traditional building methods, the cost of production and construction is quite economical.

## 2. Literature Review

### 2.1 Thin Walled Cold-formed Steel

Cold-formed steel members were first used in building construction in the middle of the 18th century. However, it wasn't until the 19th century when CFS were commonly used in building construction (Institute, 2010). There are two major types of structural members in the world of steel construction. The first is the class of members and forms that are hot-rolled from plates. The second category of steel is called cold-formed steel, and it is made up of

cold-formed sections made from steel sheet, strip, plate, or flat bar using press brake or bending brake operations, as well as roll-forming equipment (Yu & W.-w. & LaBoube). According to him in Europe, the typical thickness of steel sheets or strips used in cold-formed steel structural members is between 0.4 and 4 mm and structural structures can be formed into cold formed members from steel plates and bars as thick as 25.4 mm. Many cold-formed steel products are available in the market that are extensively utilized in building construction; some of these items are coated, while others are uncoated, depending on the purpose for which they are used. Two primary categories can be used to categorize cold-formed steel elements: panels & decks and individual structural frame members (Dubina, 2012). Cold formed steel sections have a very small thickness in relation to their width. They are therefore more likely to buckle. CFS sections buckle before yielding when subjected to an applied compression force. Therefore, it is crucial to take buckling into account when creating specs for structural and non-structural CFS parts (Billah, 2014). Shear, distortional, global, and local buckling are the four primary types that can occur. Local buckling is the most common kind of buckling for CFS components. The comparatively short wavelength of a single plate member indicates local buckling. Global buckling, however, also includes later-torsional buckling of beams and flexural-torsional buckling of columns. The body as a whole is not as much deformed by the cross section when flexural buckling happens. Another type of buckling is called distortional buckling, where the distortion wavelengths are in the middle. This can be easily calculated by using CUFSM software, creates signature curve section from where half wavelength of buckling can be found (B.W. Schafer1 and S. Ádány, 2006). In compression test if five times the length of short wavelength (minima) of buckling is used it can incorporate the effects of that buckling in test (Li Li Wu, 2006). The buckling failures of cold-formed steel profiles are commonly caused by the members' compression, shear, and bending loads.

### 3.2. Double Corrugation

The present-day building industry usually utilizes innovative production and assembly technologies to ensure reliability and ease of construction of complex and simple structures. Additionally, k-span arch structures are the most frequently used building material globally, especially in roofing and cladding. Thus, the k-span arch profile is usually used in the construction industry nowadays because of its simple and quick method of fabrication and quick installation. The research study by (A. Piekarczuk, 2021) (Artur Piekarczuka, 2019) (Li Li Wu, 2006) (Robert Cybulski a, 2014) focused on recent studies based on analyses of double corrugated arch structure (k-span system arch) to validate the current scientific research possibilities of newly adopted measurement systems along with efficiency and reliable numerical computational techniques.

Moreover, k-span system arch profiles need better-founded design techniques, so these design challenges in production contribute to failures and buckling of structural members. Recently, k-span systems have been found in various variations worldwide, especially in the construction sectors. Several k-span system variations are manufactured with the Automatic Buildings Machine (ABM). Similarly, The ABM creates numerous types of profiles with different cross-section shapes. Although ABM 240 and ABM 120 are the most frequently used in the construction industry and both k-span system profiles are shown in Figure 4 & 5 (A. Piekarczuk, 2021).

Fundamentally, the ABM 240 (Roye, 1997) version is utilized to develop a circular arch profile with a spa of up to 36m. In contrast, ABM 120 version generates circular arch profiles of 24m span length. Moreover, the

manufacturing and integration processes of both versions are similar. Each variation consists of numerous modifications with different shapes, corrugation types, size of the tray profile, and application range depending on the specified arch span and rise, even though the previously mentioned k-span variations share similar features with transverse ribs on the wed surface, which are formed in the second stage rolling process. Currently, the significant challenges facing the utilization of the k-span system profile are because of various difficulties regarding the need for more standards in computational methods. Similarly, the recent features of k-span system profiles have no specified standards for an application that covers surface shape features in European standards (Piekarczuk, 2021; Dubina, 2002; Dubina, 2012; EN 1993-1-1: Eurocode 3, 2005; EN 1993-1-5: Eurocode 3, 2006; Eurocode 1 Part 1–4; Wu, 2006; Robert Cybulski, 2014; Biegus, 2013; Airumyan, 1997). Furthermore, the local buckling failures indicate there is an urgent need to consider the specificity of k-span profiles application in the construction sector, thereby utilizing applicable scientific research and numerical methods (A. Piekarczuk, 2021).

**Figure 3 (K-Span Jointing) (A. Piekarczuk, 2021)**

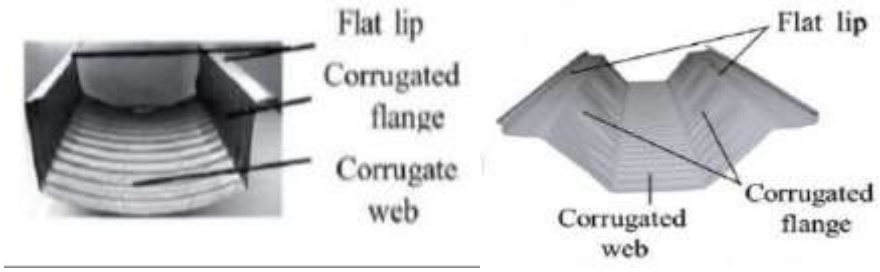


**Figure 4 (K-Span Profiles)**

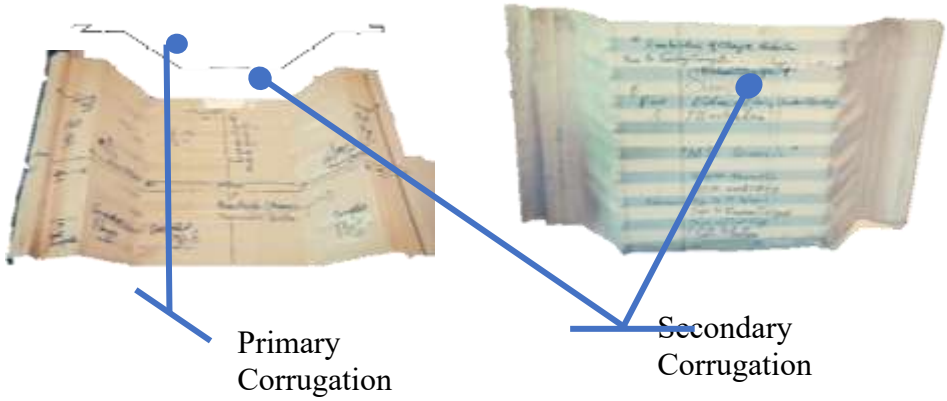


**Figure 5 (K-Span Profiles)**

### 3.3. Collapses in recent past

There are some collapses in recent past in different areas of Europe as shown in Figures 6 & 7. Profiles with transversal corrugation are not covered by European standards pertaining to the design of steel thin-walled elements. Insufficient instruments to accurately evaluate those structures' ability to support loads. The majority of the time, the design process relies on common information rather than specialized knowledge of the structure's unusual traits. Failures might result from inadequate understanding of the double corrugated structure design guidelines (Biegus, 2013; Mang). The complex structural geometry of the double corrugated roof structure, these days, is analyzed by different computer software i.e., ANSYS, LS-DYNA, ABAQUS using finite element method FEM (Chen, March 5, 2018).

### 3.4. Finite Element Analysis (FEA)

The Finite Element Method (FEM) has been the most versatile numerical technique used for the simulation and modeling of advanced engineering systems FEM has become an indispensable technique and standard tool for effectively developing a system and for cost effectiveness in the fabrication process (Erhunmwun, 2017; Becker, 2001; Li Wu, 2006; Chen, 2018; Zaraś, 2001).

#### 3.4.1. ANSYS Static Structural Analysis

A static structural analysis is one of the many analysis systems of ANSYS Workbench used to determines the effect of steady (or static) loading conditions on a structure, while omitting inertia and damping effects, such as those caused by time varying loads (Mang, H.A; Mang, 2018). The general robust procedure and features involved in Finite element analysis can be summarized in seven different steps below:

- Generate boundary conditions (mathematical modelling) and governing equations for the problem.
- Discretization (meshing) of geometry domain into finite pieces called elements.
- Formulation of element equations (algebraic equations) and selection of interpolation function (shape function)
- Assembly of all the element equations to an obtained system of equations for the entire model
- Applying boundary conditions and loads.
- The Solution of the system global equations or algebraic equations for nodal displacement)
- Presentation and interpretation of the simulation results in tabular form, curves, and graphical plots.

**Figure 6 (View of the store hall in Gdansk (Poland) after collapse) (A. Biegus, 2013)**

**Figure 7 (Yuzhno-Sakhalinsk (Russia) (A. Piekarczuk, 2021)**

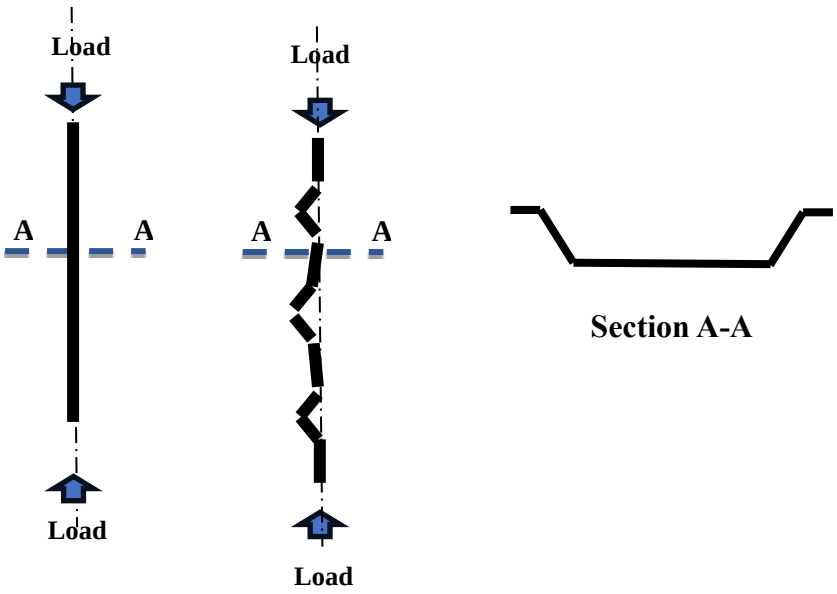


**Figure 8 (Load Transfer in compression)**

## 3. Methodology

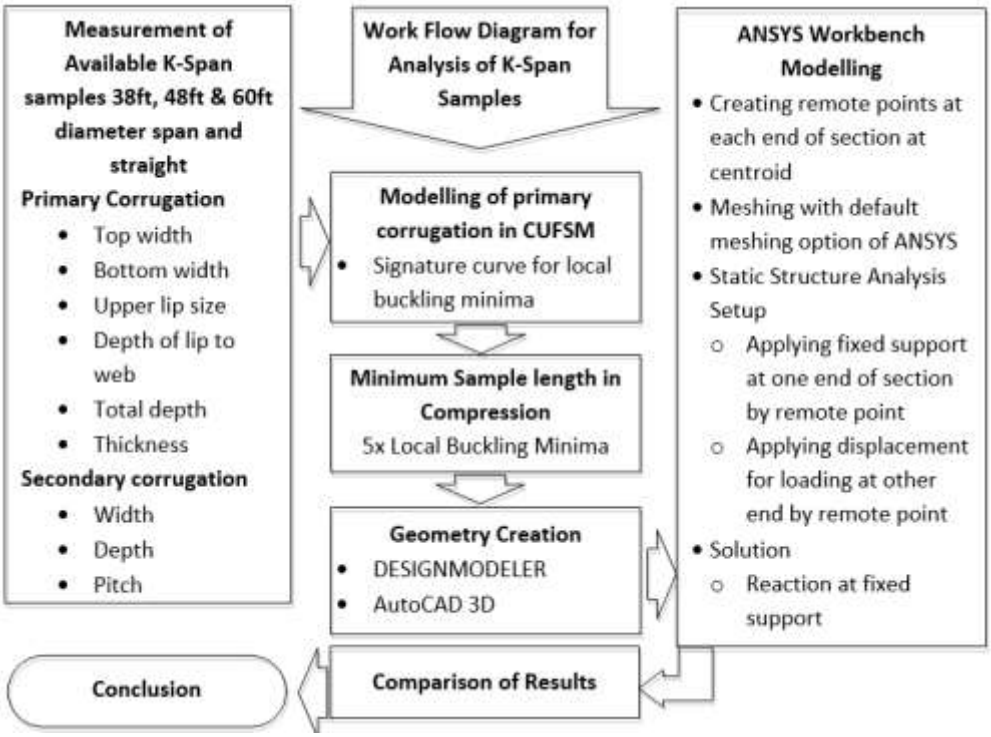


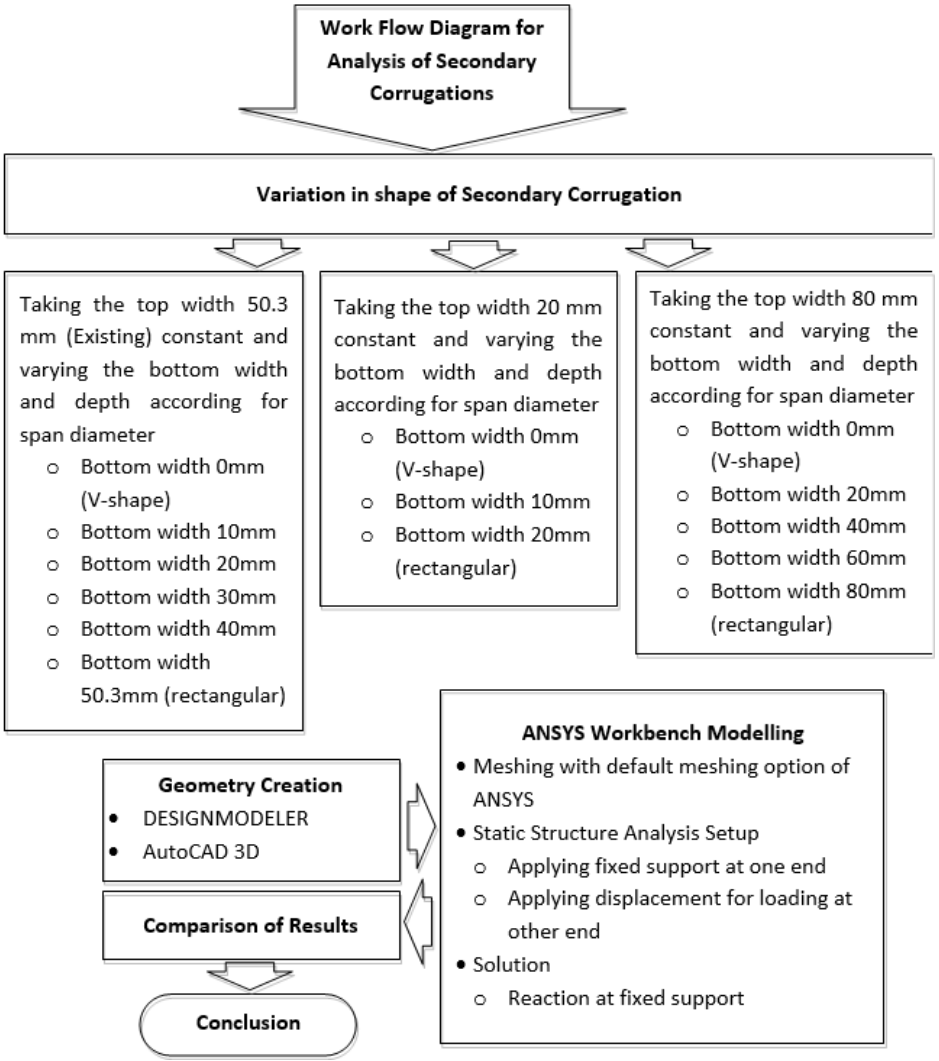

### 3.1 Sample

Samples from straight profile, 38ft, 48ft and 60ft diameter span length were taken and measurement of profile was done as shown in figure 9 and table 1. To check the minimum size of sample for compression to incorporate the local buckling effects in testing, the straight sample was modelled in CUFSM software and signature curve was obtained which showed that the local buckling minima is 52mm as shown in figure 10. So, sample length was taken five times the local buckling minima which comes out to be 260mm (5 times 52mm).

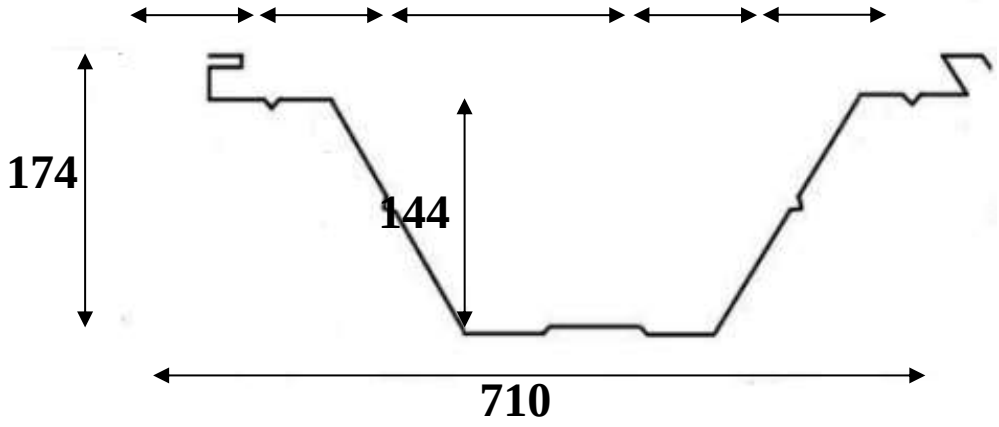


**Figure 9 (Trapezoidal Test Sample)**

**Table 1 (List of Samples)**

| Sr# | Sample | Thickness (mm) | Sample Length (mm) |
|---|---|---|---|
| 1 | **Trapezoidal straight** | 0.6 | 260 |
| 2 | **Trapezoidal 38ft Diameter** | 0.6 | 260 |
| 3 | **Trapezoidal 48ft Diameter** | 0.6 | 260 |
| 4 | **Trapezoidal 60ft Diameter** | 0.6 | 260 |

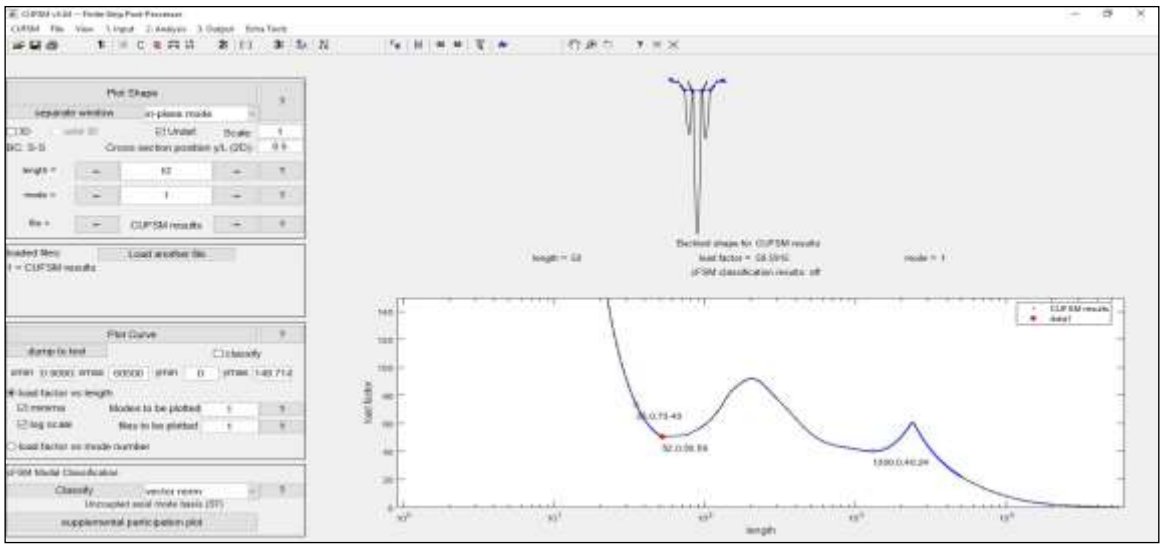

**Figure 10 (Signature curve for K-span section)**

## 3.2 Finite Element Modelling of K-Span Steel Specimen

### 3.2.1 Geometry Modelling

AutoCAD 3D 2021 and ANSYS R19.2 DESIGNMODELER were used to make geometry for the samples. Firstly, actual measurements of all samples were made for both primary corrugation and secondary corrugation separately. Primary corrugation and width of secondary corrugation are same for every arch, only the depth of secondary corrugation is varying which changes

the angle to convert a straight profile into an arched profile. Table-2 shows the mathematical calculations of depth of secondary corrugations for each diameter span length. Column 1&2 shows the diameter, column 3 is the depth of main profile excluding the upper lip portion. Column 4 is the circumference according for column 2. Column 5 is the circumference according to outer diameter which is column 2 + column 3. Column 6 calculates the difference between outer and inner circumference, this is the value which has to be compensated during arch forming. Column 7 is the existing width of secondary corrugation. In column 8 number of secondary corrugations are calculated from dividing the inner circumference by width of the corrugation. Column 9 calculates the depth required to compensate the value in column 6 by using Pythagoras theorem. Four number of samples with 0.6mm of core thickness were taken for modelling, one is straight profile (the primary corrugation), and other three are the arched profiles with diameter & span lengths of 38ft, 48ft and 60ft. Measurement of primary corrugation, shown in figure 9, and secondary corrugations were done for each profile to accurately model the arch. The mains two measurements in secondary corrugation are its top width (which is fixed 50.3mm) and depth (which varies according of diameter of arch). So, calculation for depth of secondary corrugation for each sample was done to eliminate the error in measurement. The depth of secondary corrugations measured, during measurement, was within 10% of calculated. So, the calculated values were taken for modelling of geometry as shown in figure 11.

#### 3.2.2 Model Meshing

After geometry, meshing was done by ANSYS default meshing option.

#### 3.2.3 Loading and Boundary Condition

Loading and fixed support were applied to the opposite ends of sample by applying remote point option. Remote point generated a centroid of the profile which is horizontal mid-point and 78mm from bottom edge. Loading was applied by the applying displacement of 5mm in compression, which was applied in steps with minimum 10 sub-steps for each. Reaction force at fixed support was check to make a load deflection diagram.

**Table 2. Depth of secondary corrugation**

| Sample # | Diameter | | Depth of sample from upper lip to corrugated web | Circumference | | Difference | width of secondary corrugation | Number of secondary corrugations | Depth of secondary corrugation | | | |
|---|---|---|---|---|---|---|---|---|---|---|---|---|
| | | | | Inner | Outer | | | | Calculated | Actual | Diff. | %age Diff. |
| | ft | m | mm | m | m | mm | mm | | mm | mm | mm | |
| | 1 | 2 | 3 | 4 | 5 | 6 | 7 | 8 | 9 | 10 | 11 | 12 |
| 1 | 60.00 | 18.29 | 144.00 | 57.42 | 58.33 | 904.32 | 50.30 | 1141.57 | 4.48 | 4.20 | 0.28 | 6.27 |
| 2 | 48.00 | 14.63 | 144.00 | 45.94 | 46.84 | 904.32 | 50.30 | 913.28 | 5.01 | 4.60 | 0.41 | 8.27 |
| 3 | 38.00 | 11.58 | 144.00 | 36.36 | 37.27 | 904.32 | 50.30 | 722.95 | 5.64 | 5.80 | -0.16 | -2.77 |

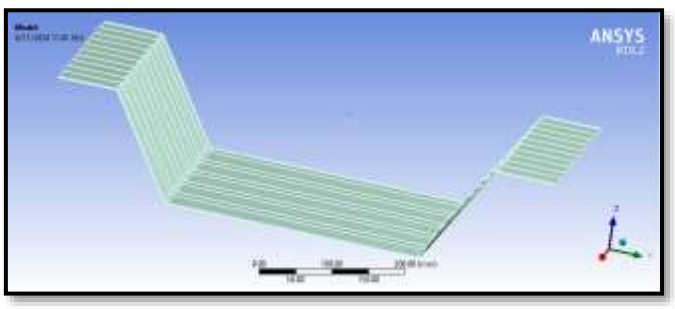


**Figure 11 (Sample Model)**

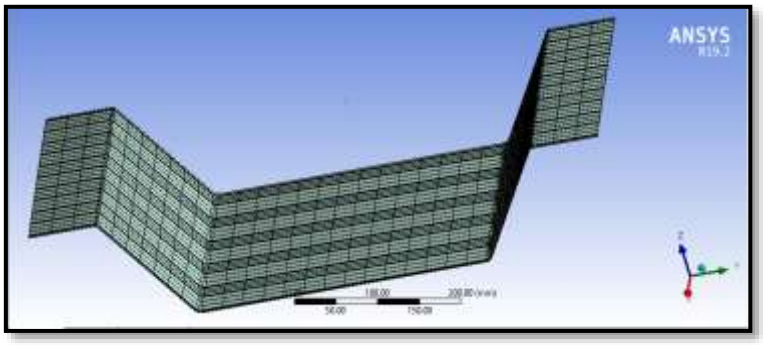


**Figure 12 (Meshing)**

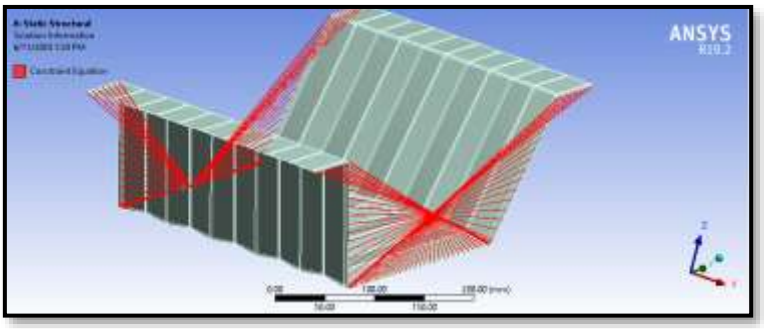


**Figure 13 (Centroid point for loading and fixed support)**

### 3.2.4 Results and Discussion

Compression test on samples in ANSYS clearly shows that as the diameter of the arch increases the depth of secondary corrugation increases which increases the load carrying capacity of the section as shown in figure 22. As already many researches shown similar kind of results (Li Li Wu, 2006) (Robert Cybulski a, 2014). In figure 14 the result of compression test on straight profile without secondary corrugations, in comparison to figure 22 (load-displacement curves of arched profiles), clearly shows that the straight profile has greater resistance to deformation, greater load carrying capacity but lesser ductility. It showed around 40% more load carrying capacity than the arched profiles. Figure 16 shows the load carrying capacity of 38ft diameter span sample and figure 17 shows its deformation shapes, the peak load is 64,253N at 4.5mm displacement (applied displacement) in X-direction. In figure 17D the total deformation is shown, which indicates the out of plane buckling in central part of web and upper lip portion are the dominating deformations. Figure 17A, 17B & 17C shows the deformation in x, y and z directions respectively.

The load carrying capacity of 48ft diameter span sample and its deformation shapes are shown in figure 18 & 19 respectively. The peak load is 65,133N at 4.53mm displacement (applied displacement) in X-direction. In figure 19D the total deformation is shown, which indicates the out of plane buckling in central part of web and upper lip portion are the dominating deformations, in comparison to figure 17D the buckling in upper lip is increased and deformation is distributed greater portion of web. Figure 19A, 19B & 19C shows the deformation in x, y and z directions respectively. Figure 20 & 21 gives the load carrying capacity of 48ft diameter span sample and its deformation shapes respectively. The peak load is 69,364N at 4.6mm displacement (applied displacement) in X-direction. Figure 21C is shows distribution, of buckling in z-direction, in wider area rather than concentrated at some small portion. And load carrying capacity is also increased in comparison to 38ft & 48ft diameter span samples. In figure 21D the total deformation is shown, which indicates the out of plane buckling in central part of web and upper lip portion are the dominating deformation. Figure 19A, 19B & 19C

shows the deformation in x, y and z directions respectively. The comparison of load carrying capacity of 38ft, 48ft and 60ft diameter span sample are shown in figure 22. As diameter increases the samples showed different kind of failure shape. 38ft diameter sample showed buckling of main web and local buckling of upper lips, 48ft diameter sample showed increase upper lip local buckling, and 60ft diameter sample showed the wide spread deformations in greater portion.

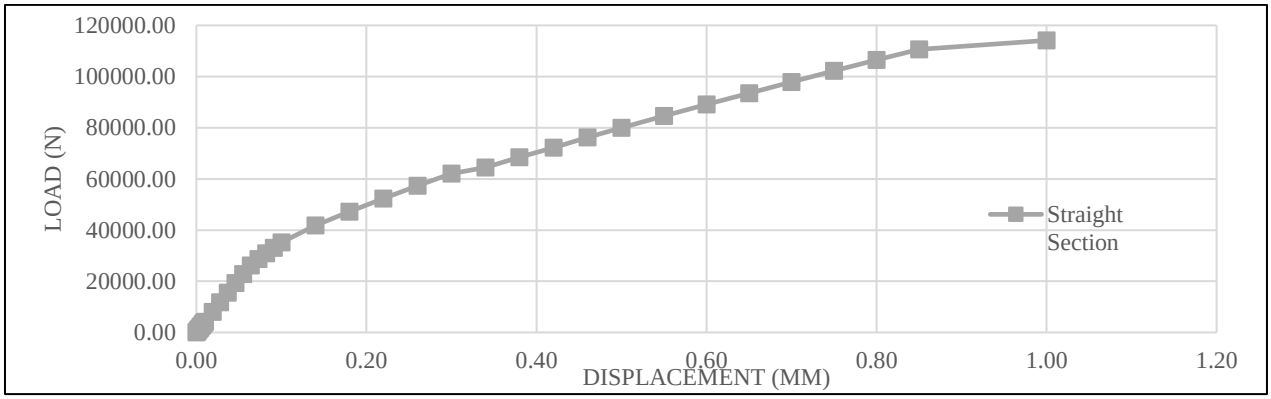


**Figure 14 (Compression Testing on ANSYS Results Straight section Load - Deflection Graph)**

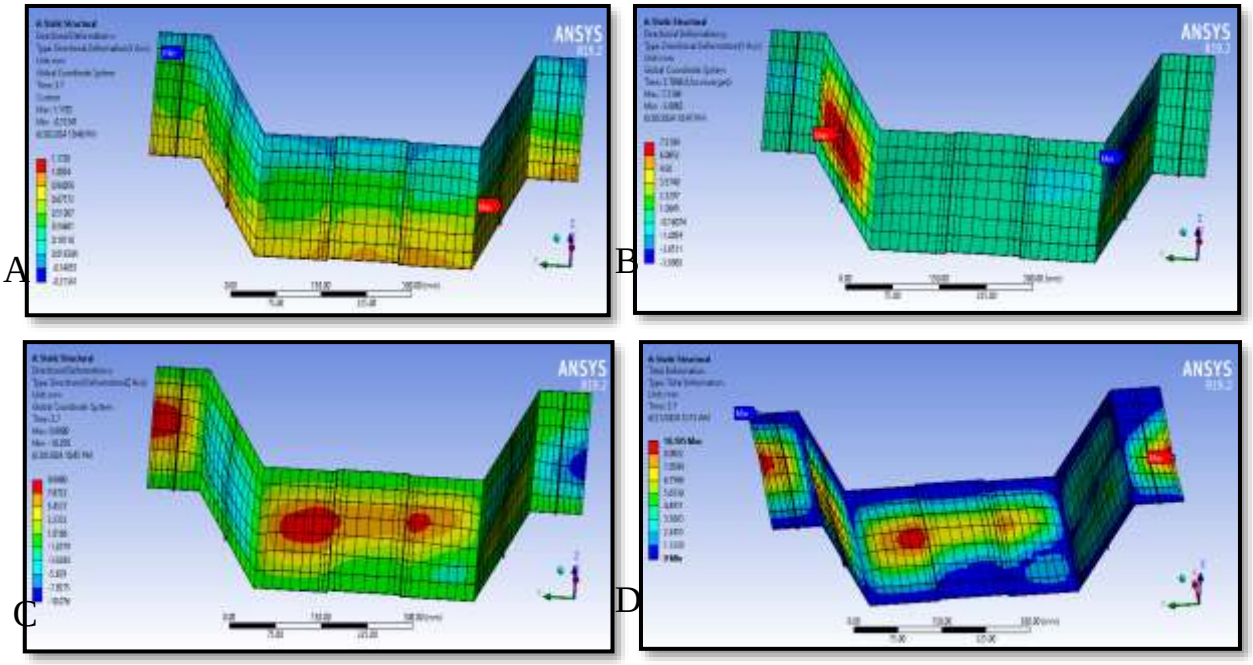


**Figure 15 (Deformation Shape of straight sample (A-X direction, B-Y direction, C-Z direction, D-Total))**

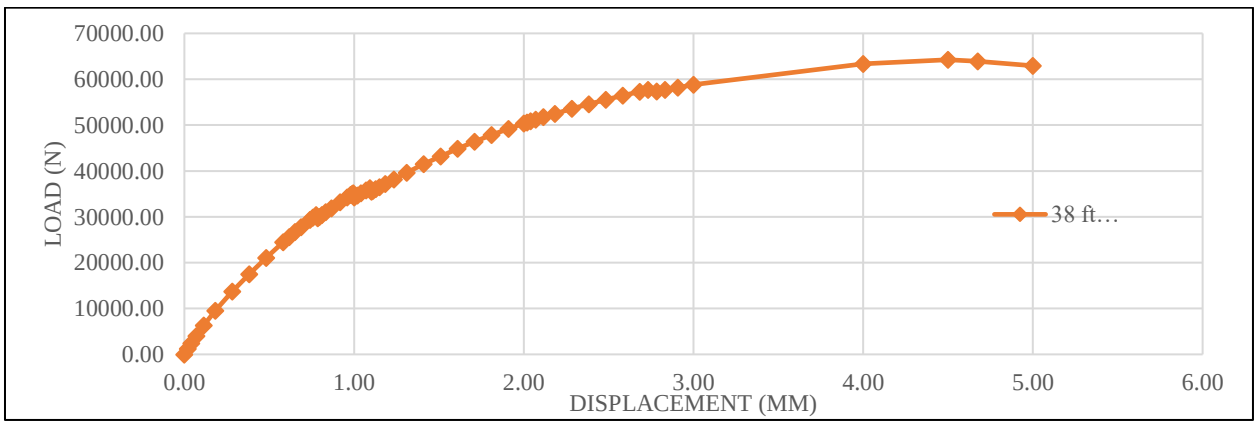


**Figure 16 (Compression Testing on ANSYS Results of 38ft diameter k-span Load - Deflection Graph)**

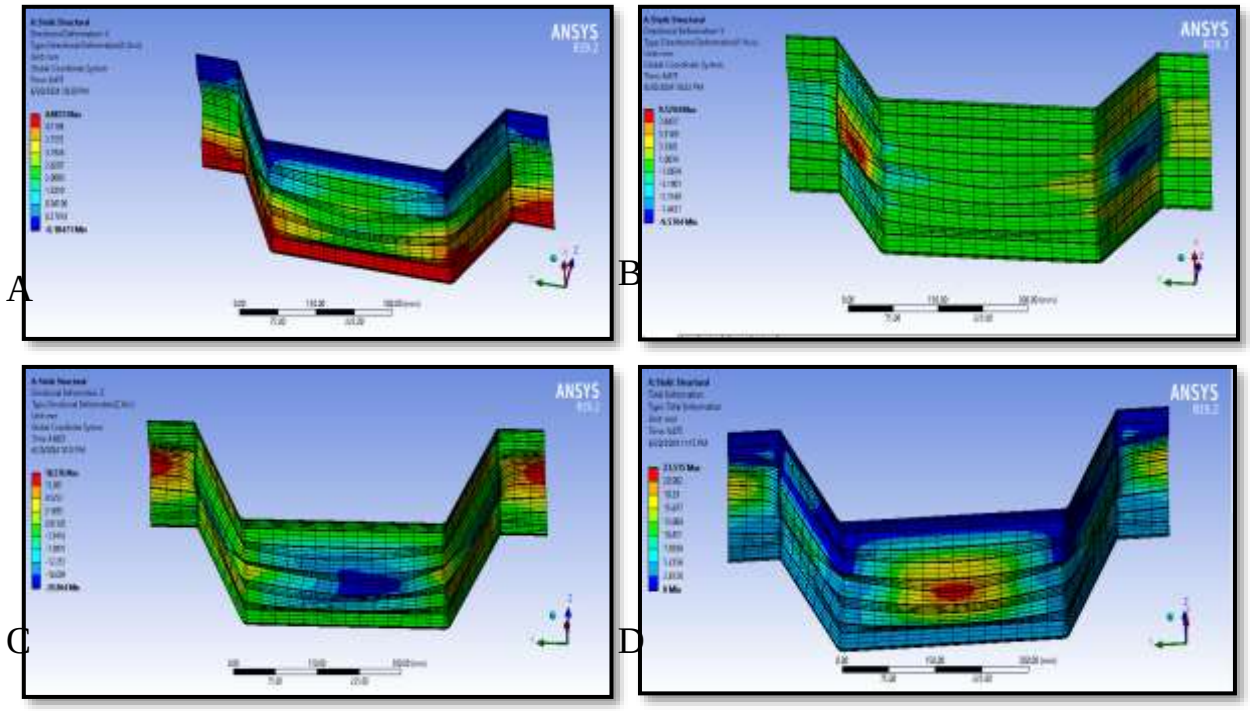


**Figure 17 (Deformation Shape of 38ft diameter k-span sample (A-X direction, B-Y direction, C-Z direction,** D-Total))

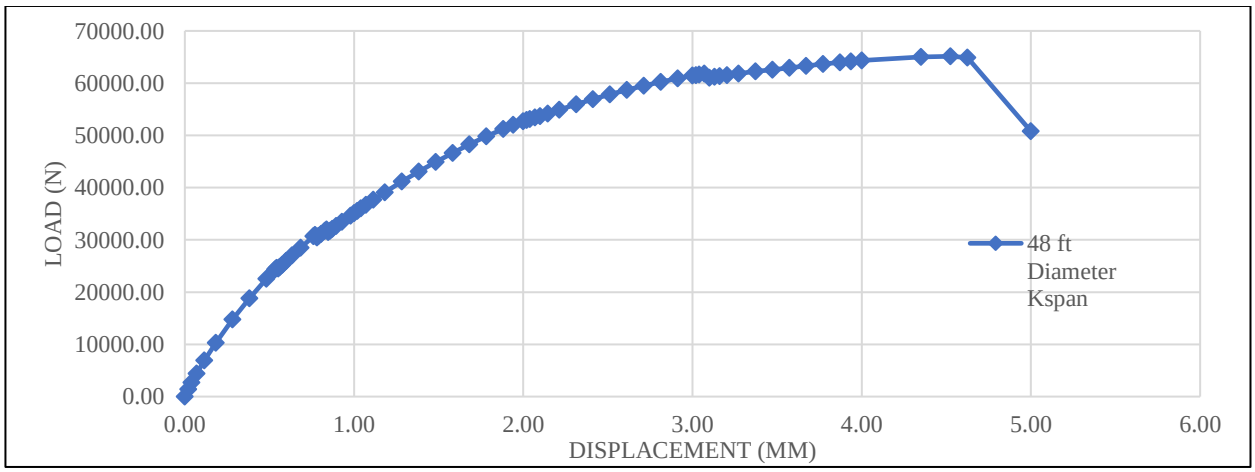


**Figure 18 (Compression Testing on ANSYS Results of 48ft diameter k-span Load - Deflection Graph)**

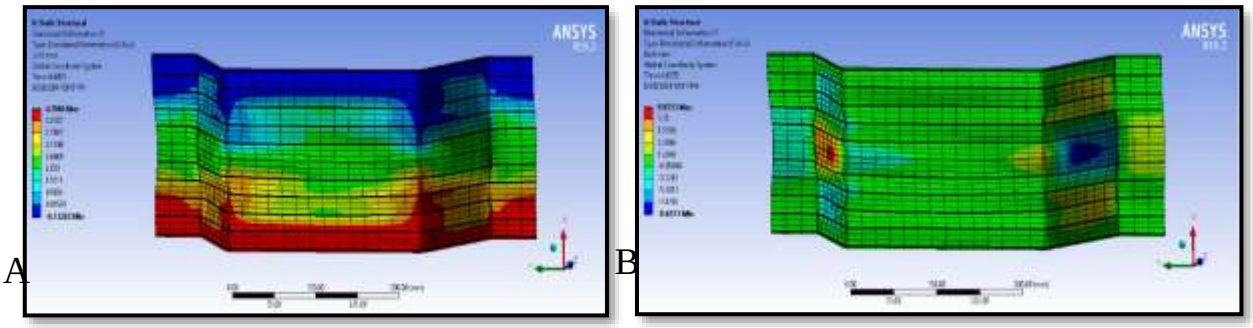

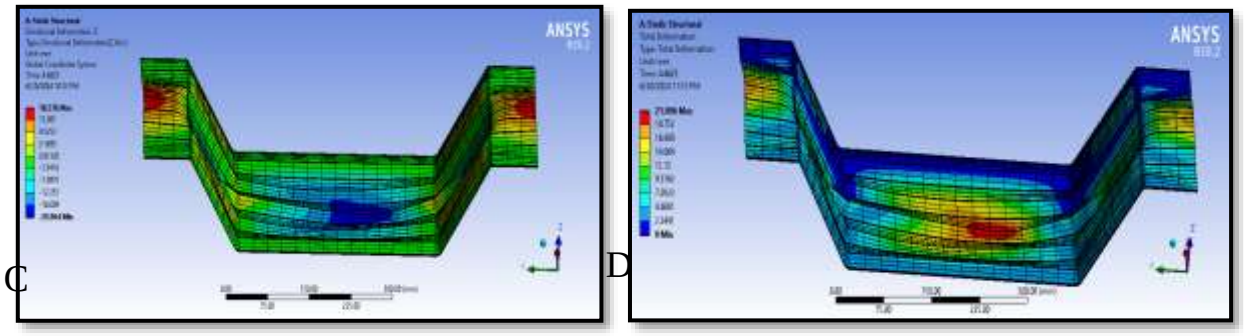


**Figure 19 (Deformation Shape of 48ft diameter k-span sample (A-X direction, B-Y direction, C-Z direction, D-Total))**

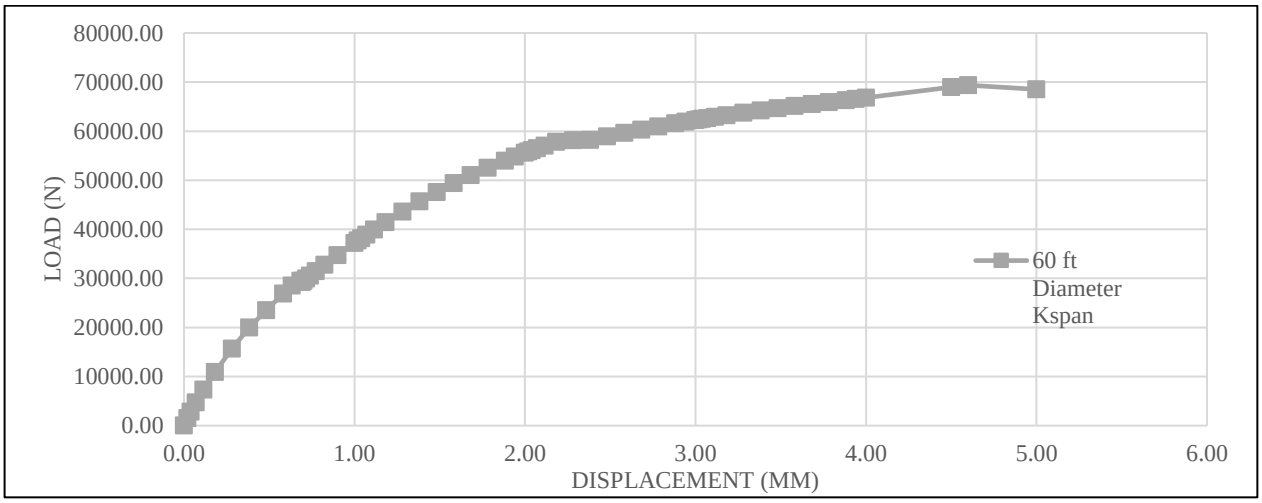


**Figure 20 (Compression Testing on ANSYS Results of 60ft diameter k-span Load - Deflection Graph)**

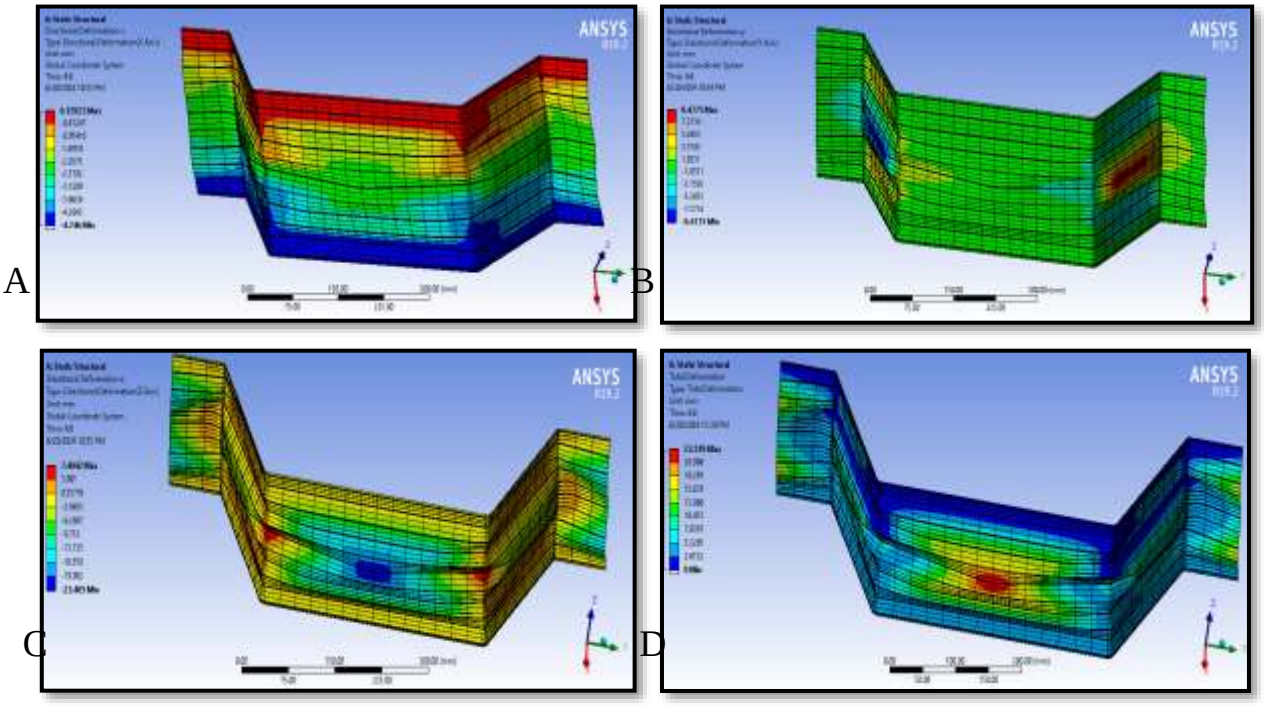


**Figure 21 (Deformation Shape of 60ft diameter k-span sample (A-X direction, B-Y direction, C-Z direction,** D-Total))

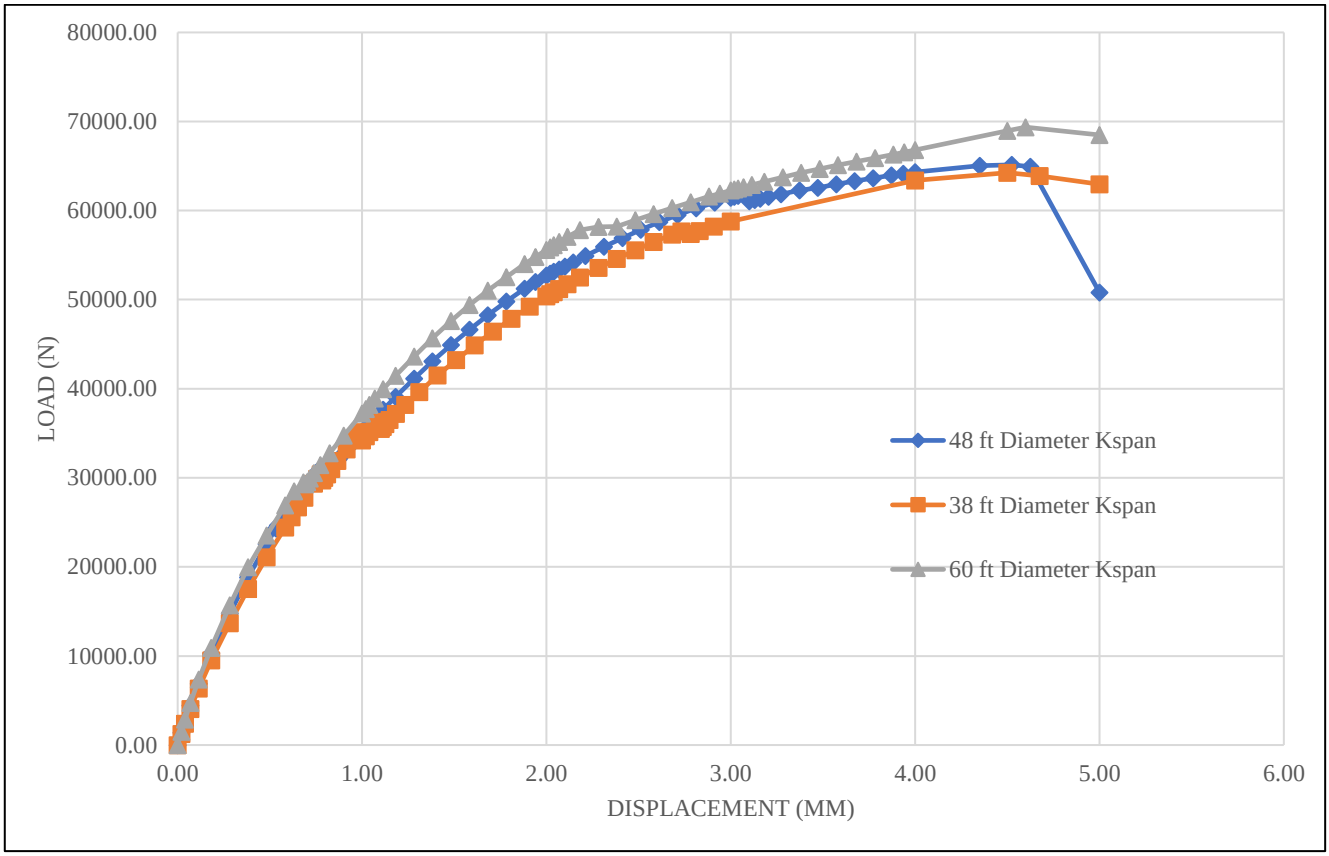


**Figure 22 (Compression Testing on ANSYS Results Comparison Load - Deflection Graph)**

### 3.3 Finite Element Modelling of Secondary Corrugations

Results shown by k-span samples are the effects of change in width and depth of secondary corrugation. Some researchers have done testing on k-span samples with same V-shape secondary corrugations no work has been done on variation in shape and size of secondary corrugation.

In this section different sizes and shapes of secondary corrugations are evaluated based on modelling in ANSYS Workbench. Three types of variations were evaluated as follows;

- Keeping the top width of the secondary corrugation same as per existing profile, i.e., top width 50.3mm, and changing the bottom width and accordingly depth as per 38ft, 48ft and 60ft diameter k-spans (Table 3).
- Decreasing the top width to 20mm and keeping it constant, and changing the bottom width and accordingly depth as per 38ft, 48ft and 60ft diameter k-spans (Table 4).
- Increasing the top width to 80mm and keeping it constant, and changing the bottom width and accordingly depth as per 38ft, 48ft and 60ft diameter k-spans (Table 5).

Sample of length 260mm, same as k-span, was modelled on AutoCAD and ANSYS as shown in figure 23. Meshing was done by ANSYS default meshing option which has given a clear and smooth mesh as shown in figure 24.

One end of sample was fixed and displacement at opposite end was applied, direction of loading is in y-direction as per figure 23. Reaction at fixed end was calculated and load deflection curve was plotted.

**Table 3 Secondary Corrugation Depths for Different bottom width and constant top width of 50.3mm**

| Secondary Corrugation Depths for Different bottom width and constant top width 50.3mm | | | | | |
|---|---|---|---|---|---|
| V shape | Bottom Width 10mm | Bottom Width 20mm | Bottom Width 30mm | Bottom Width 40mm | Rectangular |
| mm | mm | mm | mm | mm | Mm |
| 4.48 | 4.01 | 3.49 | 2.86 | 2.06 | 0.40 |
| 5.01 | 4.49 | 3.90 | 3.21 | 2.31 | 0.50 |
| 5.64 | 5.06 | 4.40 | 3.62 | 2.61 | 0.63 |

**Table 4 Secondary Corrugation Depths for Different bottom width and constant top width of 80mm**

| **Secondary Corrugation Depths for Different bottom width and constant top width 80mm** | | | | |
|---|---|---|---|---|
| **V shape** | **Bottom Width 20mm** | **Bottom Width 40mm** | **Bottom Width 60mm** | **Rectangular** |
| mm | mm | mm | mm | Mm |
| 7.13 | 6.18 | 5.06 | 3.60 | 0.63 |
| 7.98 | 6.92 | 5.67 | 4.05 | 0.79 |
| 8.98 | 7.79 | 6.39 | 4.57 | 0.99 |

**Table 5 Secondary Corrugation Depths for Different bottom width and constant top width of 20mm**

| Secondary Corrugation Depths for Different bottom width and constant top width 20mm | | | |
|---|---|---|---|
| V shape | Bottom Width 10mm | Bottom Width 20mm | Rectangular |
| mm | mm | mm | Mm |
| 1.78 | 1.26 | 0.16 | 0.16 |
| 1.99 | 1.42 | 0.20 | 0.20 |
| 2.24 | 1.60 | 0.25 | 0.25 |

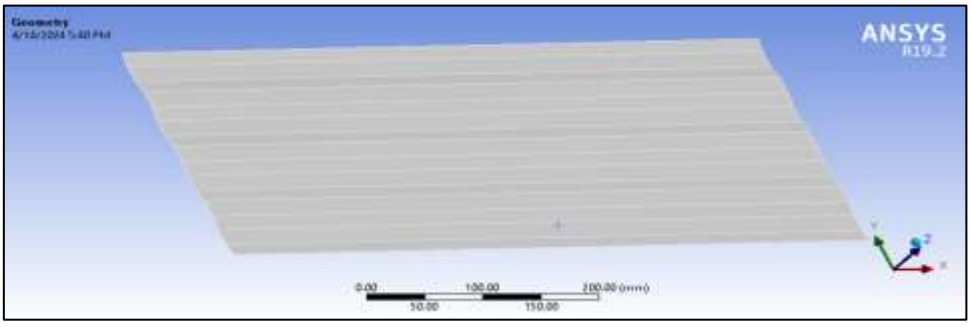


**Figure 23 (Secondary Corrugation Model)**

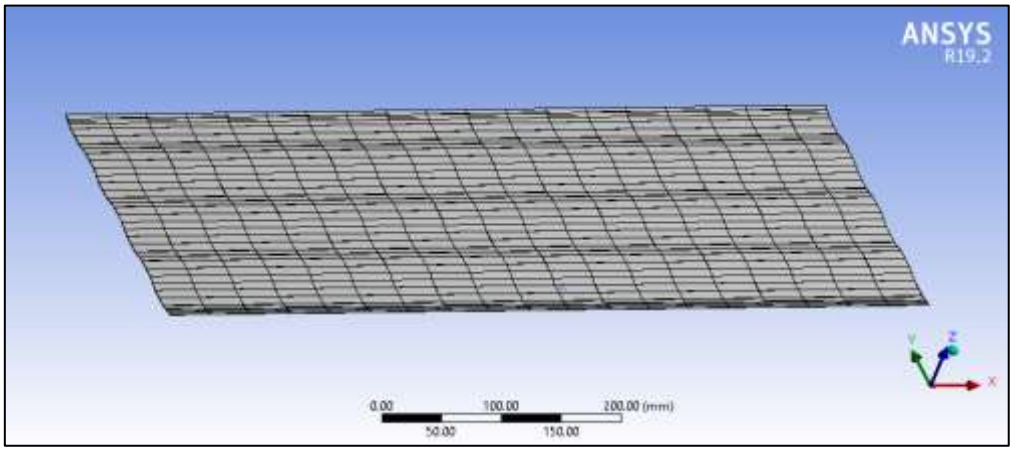


**Figure 24 (Secondary Corrugation Model-Meshing)**

### 3.3.1 Results and Discussion

- Symmetrical results have been achieved by varying the top width, bottom width and depth of secondary corrugation according to diameter.
- When the top width is kept constant 50.3 (existing) and bottom width is varied for 38ft diameter span, Figure 25 shows V-shape (existing) took around 1570N load at 1mm displacement whereas the trapezoidal shape with bottom width 40mm took more load 1663N at same 1mm displacement. Other shapes showed lower values of load than V-shape. In figure 26, top width is reduced to 20mm and kept constant by varying bottom width. The results shown that V-shape with 20mm top width took 1660N for 0.1mm displacement which is more load than V-shape with 50.3mm top width, and the displacement is 1/10th of that and showed an abrupt failure. By changing the top width to 80mm the figure 27 shows that displacement is increased to around double to that of exiting at almost same load and showed a ductile behavior.
- In figure 28, 29 & 30, the variation according to 48ft diameter span, shows the same trends as trapezoidal shape bottom width 40mm took higher load that V-shape with top width 50.3mm. Lower top width showed lower displacement values at similar load values. Higher upper width behaves in more ductile manner.
- By varying the shape of secondary corrugation for 60ft diameter span again follows the trend like 38ft and 48ft diameter. Figure 31, 32 & 33 clearly shows that shape closer to rectangular performs the best and shows greater load carrying capacity. If the top width in decreased it shows higher load to displacement value. Displacement is lower with similar load but brittle/abrupt failure occurs.
- When the shape of secondary corrugation is rectangular, results go to infinity that mean the results are un-calculated as shown in figure 34.

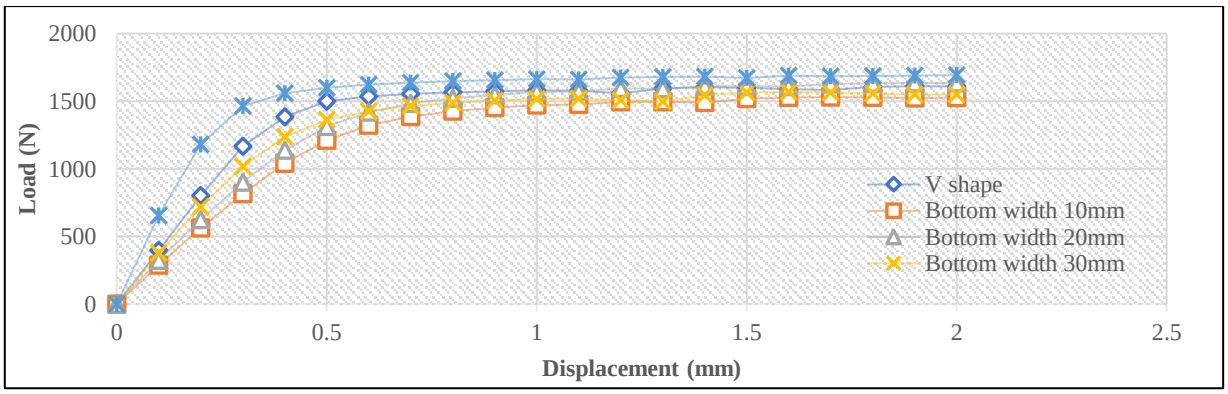


**Figure 25 (Load and Displacement Graph (According to 38 ft Diameter) Secondary Corrugation Depths for Different bottom width and constant top width 50.3mm)**

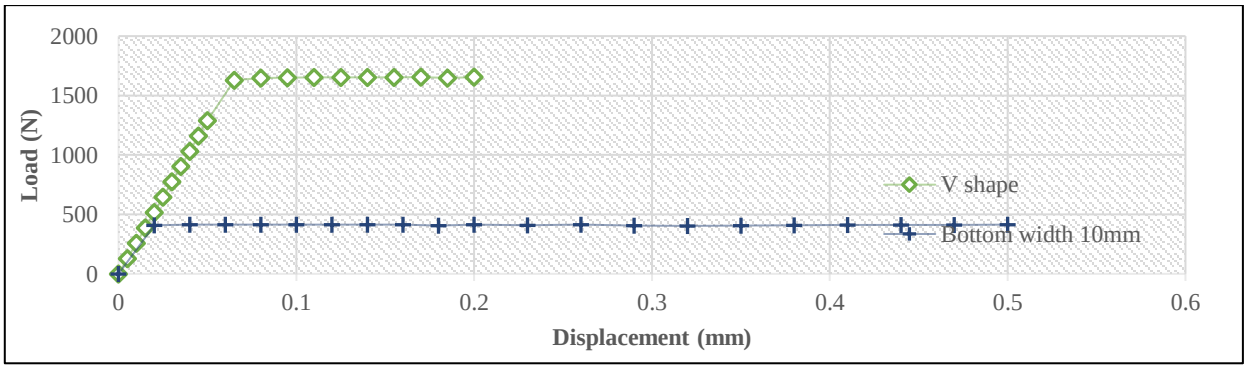


**Figure 26 (Load and Displacement Graph (According to 38 ft Diameter) Secondary Corrugation Depths for Different bottom width and constant top width 20mm)**

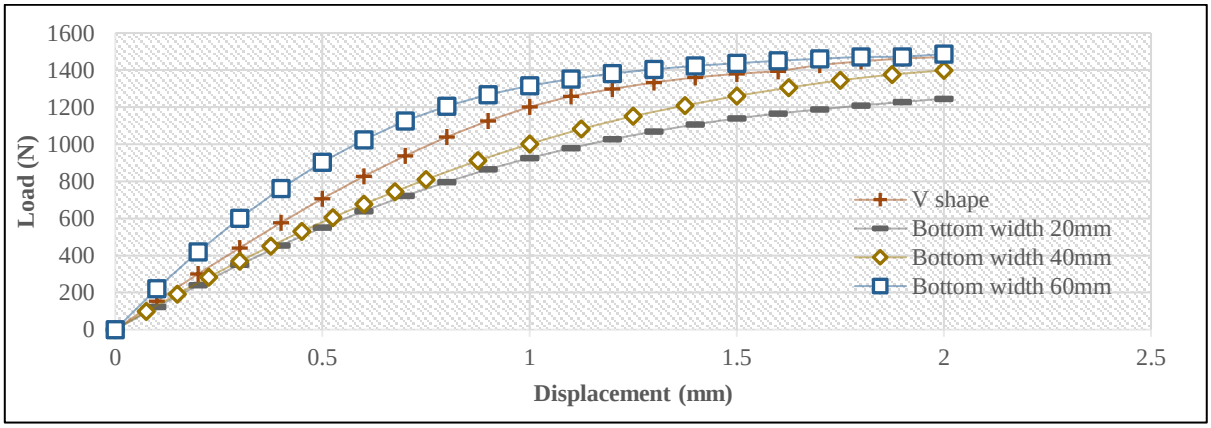


**Figure 27 (Load and Displacement Graph (According to 38 ft Diameter) Secondary Corrugation Depths for Different bottom width and constant top width 80mm)**

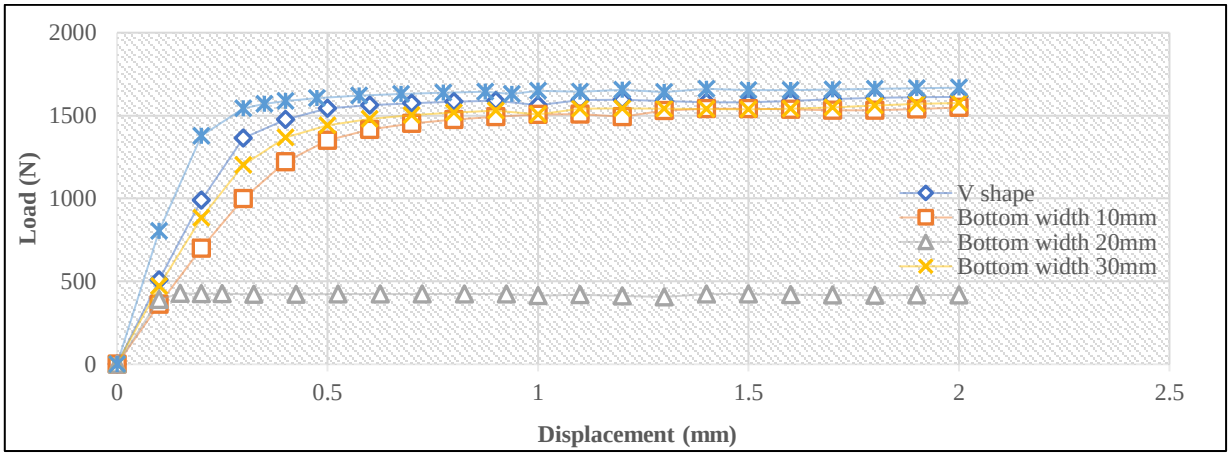


**Figure 28 (Load and Displacement Graph (According to 48 ft Diameter) Secondary Corrugation Depths for Different bottom width and constant top width 50.3mm)**

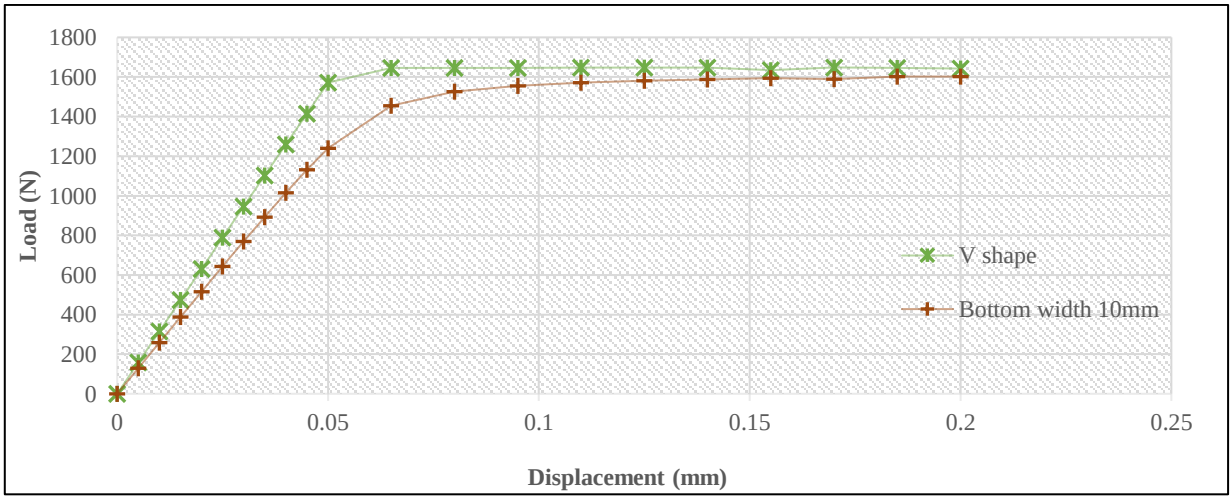


**Figure 29 (Load and Displacement Graph (According to 48 ft Diameter) Secondary Corrugation Depths for Different bottom width and constant top width 20mm)**

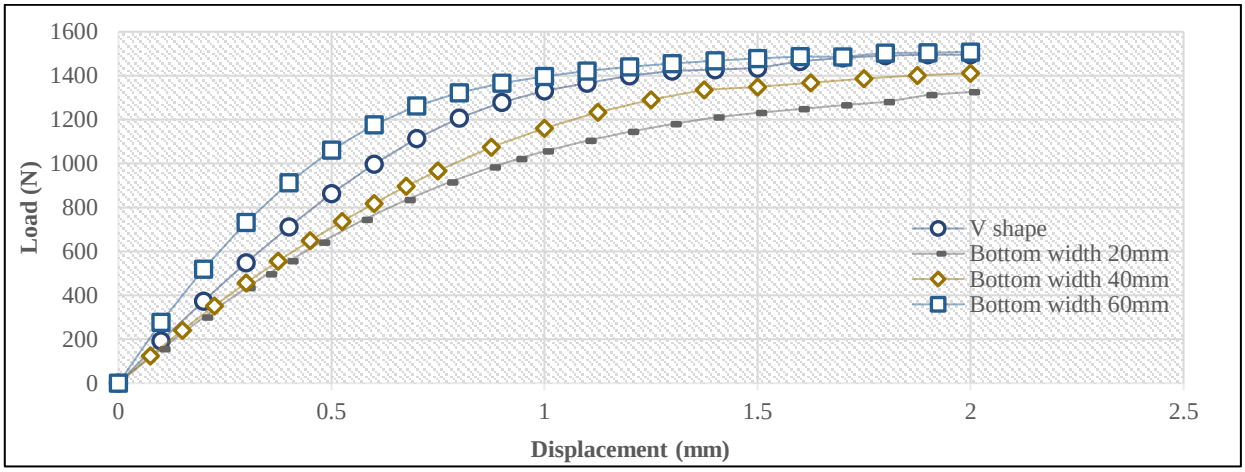


**Figure 30 (Load and Displacement Graph (According to 48 ft Diameter) Secondary Corrugation Depths for Different bottom width and constant top width 80mm)**

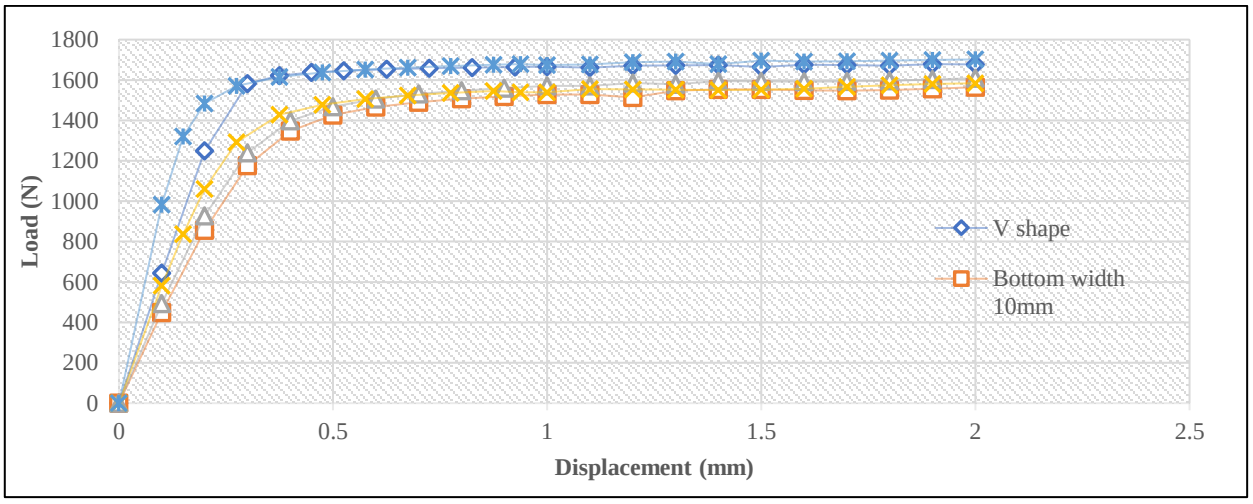


**Figure 31 (Load and Displacement Graph (According to 60 ft Diameter) Secondary Corrugation Depths for Different bottom width and constant top width 50.3mm)**

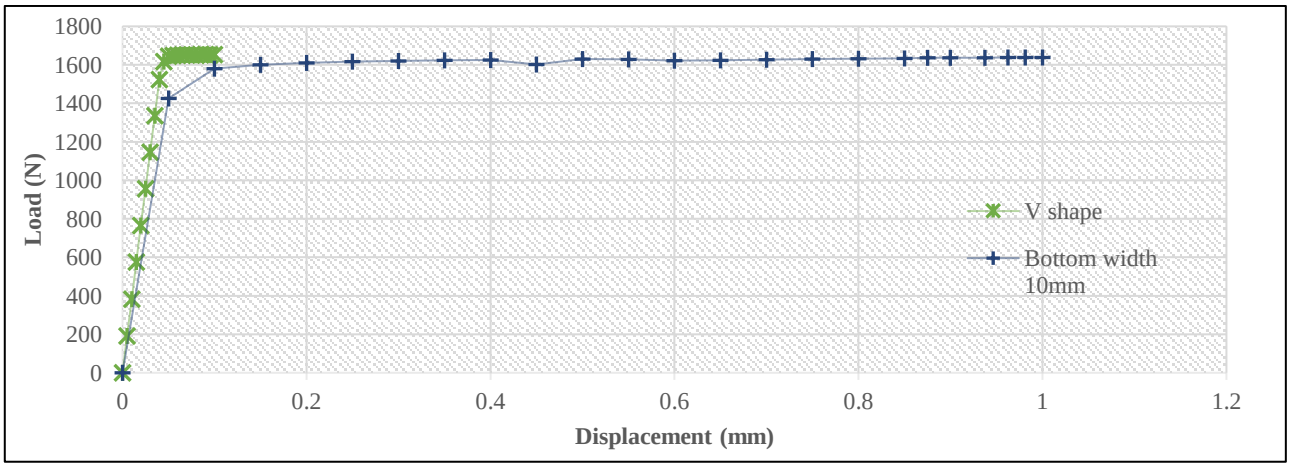


**Figure 32 (Load and Displacement Graph (According to 60 ft Diameter) Secondary Corrugation Depths for Different bottom width and constant top width 20mm)**

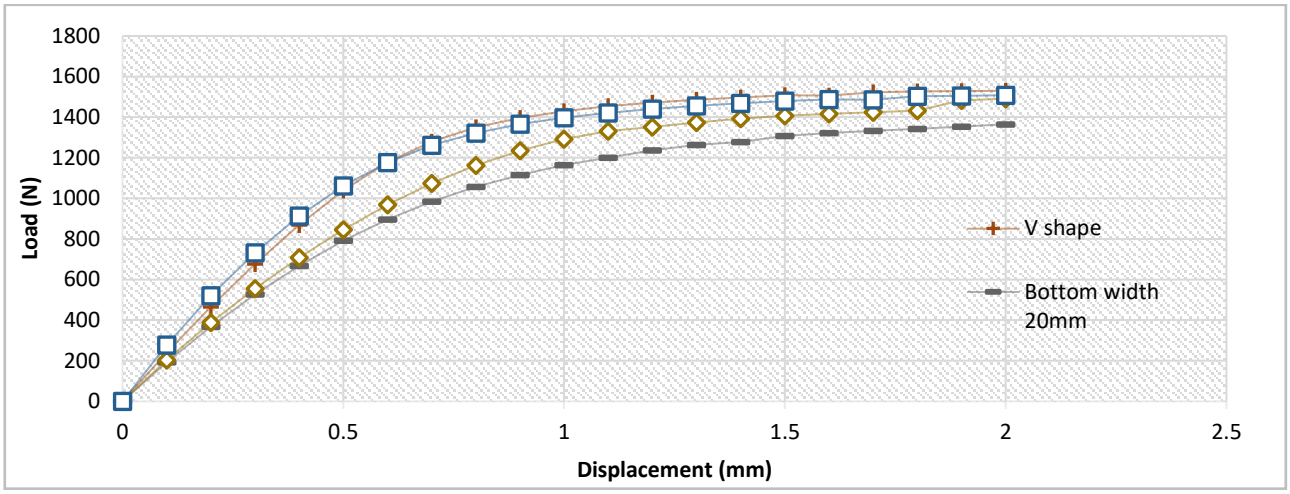


Figure **33 (Load and Displacement Graph (According to 60 ft Diameter) Secondary Corrugation Depths for Different bottom width and constant top width 80mm)**

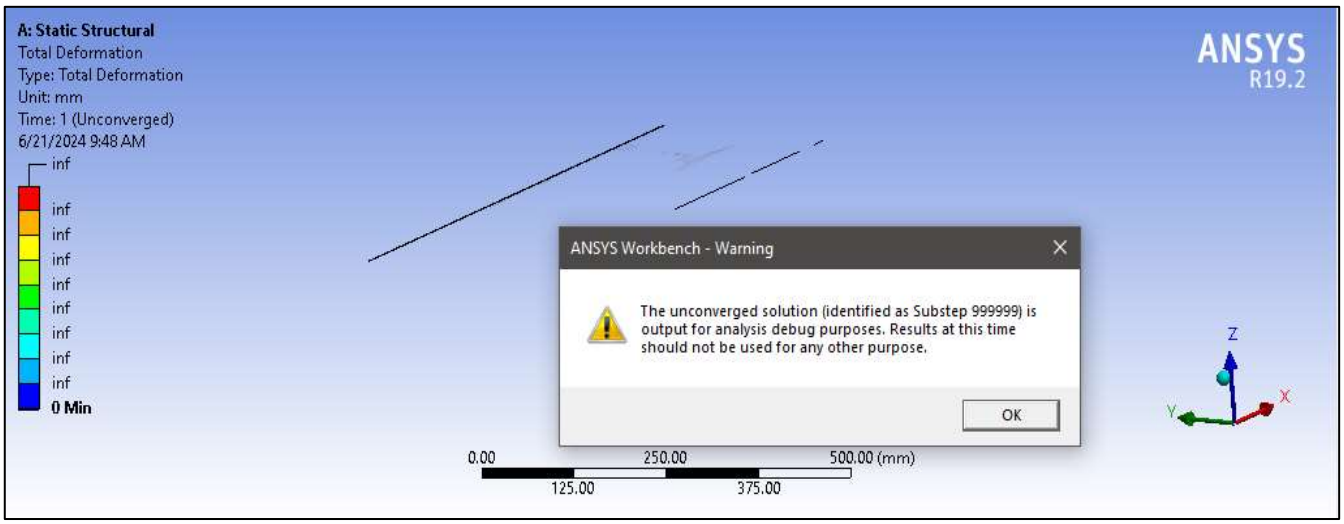


**Figure 34 (Rectangular shape Secondary Corrugation Deformation Result)**

## 4. Conclusion

- Secondary corrugation reduces the compression load carrying capacity but it is necessary to convert straight section into an arch.
- Trapezoidal shape with lower depth and internal angle (i.e., closer to rectangular shape) is the best shape for secondary corrugation according to the results of load displacement values, it takes up-to 10% more load that existing V-shape.
- Top width of around 50mm is appropriate for secondary corrugations, have ductile behaviour with good load carry capacity.
- Secondary corrugation with lower top width, 30mm less than the existing 50.3mm, has greater load to displacement ratio of around 10 times and shows less warning to failure (brittle failure).
- Secondary corrugation with higher value of top width, 30mm more than the existing 50.3mm, shows 10 % less load value and two times more displacement.
- Experimental investigation of physical samples of full-scale k-span profile, having secondary corrugation of trapezoidal shape with lower depth and internal angle, need to be done in future researches to check the overall behaviour of the structure.

- Experiments can be done, in future, on the physical samples of rectangular shape of secondary corrugation to check the performance.

**Reference**

A. Biegus, A. K. (2013). Collapse of halls made from cold-formed steel sheets. Engineering Failure Analysis.

A. Piekarczuk, P. W. (2021). Experimental and computational approaches to the evaluation of double corrugated arch structures. A review of the latest advancements. ARCHIVES OF CIVIL ENGINEERING.

Artur Piekarczuka, P. W. (2019). Experimental method to evaluate the load-carrying capacity of double corrugated sheet profiles. Thin-Walled Structures.

B.W. Schafer1 and S. Ádány. (2006). Buckling analysis of cold-formed steel members using CUFSM: conventional and constrained finite strip methods. 18th International Specialty Conference on Cold-Formed Steel Structures.

Becker, A. A. (2001). Understanding non-linear finite element analysis through illustrative benchmarks. NAFEMS.

Billah, M. M. (2014). Cold formed steel structure. World Scientific News, 59-73.

Chen, X. &. (March 5, 2018). Finite Element Modeling and Simulation with ANSYS Workbench. CRC Press. Retrieved https://doi.org/10.1201/9781351045872.

D. Zhadanov, V. U. (2015). Experimental Testing of an Arched Roofing Panel Made of MIC-120 Thin-walled Cold-formed Steel Profiles with Transverse Corrugations. СТРОИТЕЛЬСТВО. ПРИКЛАДНЫЕ НАУКИ. Строительные Конструкции, pp.33–38.

Dubina D, U. V. (2002). Effect of imperfections on numerical on instability behaviour of cold formed steel members. Thin-Walled Structures, 239-262.

Dubina, D. U. (2012). Part1-3: Design of Cold-formed Steel Structures. ECCS – European Convention for Constructional Steelwork.

E. Airumyan, O. B. (1997). Full-Scale Testing and Design of Frameless Arch Steel Roof. Struct. Assessment. Role Large Full Scale Test., E & FN Spon, 1997: pp. 211–217.

EN 1993-1-1: Eurocode 3. (2005). Design of steel structures - Part 1-1: General rules and rules for buildings, 2005. Eurocode 3.

EN 1993-1-5: Eurocode 3. (2006). Design of steel structures - Part 1-5: General rules - Plated structural elements, 2006. Eurocode 3.

Erhunmwun, I. D. (2017). Review on finite element method. Journal of Applied Sciences and Environmental Management https://dx.doi.org/10.4314/jasem.v21i5.30.

Eurocode 1 Part 1–4. (n.d.). Actions on structures – Part 1–4 General actions, Wind action. 2008: PN-EN 1991-1-4:2008 Eurocode 1.

Institute, A. I. (2010). Cold-Formed Steel in Building Construction. Steel.org.

J. Zaraś, K. M. (2001). A simplified Computation Model of Arch-Shaped Corrugated Shell Roof. Third Int. Conf. Thin-Walled Struct., Elsevier, 2001.

Li Li Wu, X. G. (2006). Theoretical and experimental study on interactive local buckling of arch shaped corrugated steel roof. Steel Structures, no. 6, pp.45–54, 2006.

Mang, H.A. (2018). Finite element analysis of doubly corrugated shells. Journal of the Structural Division, no. 102, http://cedb.asce.org/CEDBsearch/record.jsp?dockey=0006980.

Mang, H.A. (n.d.). Analysis of Double Corrugated Shell Structures by the Finite Element Method. Texas Tech University.

Robert Cybulski a, R. W. (2014). Local buckling of cold-formed elements used in arched building with geometrical imperfections. Journal of Constructional Steel Research.

Roye, K. L. (1997). Metal Building Construction using MIC-240 ABM K-Span Machine. Department of Civil Engineering University of Florida.

Yu & W.-w. & LaBoube, R. A. (n.d.). Cold-Formed Steel Design. John Wiley & Sons, Inc, 2010.